2011

Density and Temperature Scaling of Disorder-Induced Heating in Ultracold Plasmas

Scott D. Bergeson
Brigham Young University, scott.bergeson@byu.edu

A. Denning
Brigham Young University

M. Lyon
Brigham Young University

F. Robicheaux
Auburn University

Density and temperature scaling of disorder-induced heating in ultracold plasmas

S. D. Bergeson,[1] A. Denning,[1] M. Lyon,[1] and F. Robicheaux[2]

[1]*Department of Physics and Astronomy, Brigham Young University, Provo, Utah 84602, USA*

[2]*Department of Physics, Auburn University, Auburn, Alabama 36849, USA*

We report measurements and simulations of disorder-induced heating in ultracold neutral plasmas. Fluorescence from plasma ions is excited using a detuned probe laser beam while the plasma relaxes from its initially disordered nonequilibrium state. This method probes the wings of the ion velocity distribution. The simulations yield information on time-evolving plasma parameters that are difficult to measure directly and make it possible to connect the fluorescence signal to the rms velocity distribution. The disorder-induced heating signal can be used to estimate the electron and ion temperatures ~100 ns after the plasma is created. This is particularly interesting for plasmas in which the electron and ion temperatures are not known.

I. INTRODUCTION

Strongly coupled neutral plasmas combine elements of atomic physics, plasma physics, and condensed-matter physics [1–6]. Many of the simplifying approximations used in these different fields can be tested in strongly coupled systems. For example, the number of particles per Debye sphere can be continuously adjusted over a wide range by changing the initial electron energy and plasma density. This makes it possible to study the transition from an ideal plasma to a strongly coupled Coulomb system in a regular and highly controlled manner.

Ultracold neutral plasmas are created by photoionizing laser-cooled atoms [7–12]. Although the initial ion temperature is typically 1 mK, it rapidly increases by a few orders of magnitude due to Coulomb interactions with neighboring ions [5,10–13]. The strong coupling parameter is thereby limited to $\Gamma \approx 2$, where $\Gamma = e^2/4\pi\epsilon_0 a_{ws}k_B T$ is the ratio of nearest-neighbor potential energy to kinetic energy, $a_{ws} = (3/4\pi n)^{1/3}$ is the Wigner-Seitz radius, and n is the density. This heating mechanism, raising the ion temperature from essentially zero to near the correlation temperature

$$T_c = \frac{2}{3}\frac{e^2}{4\pi\epsilon_0 a_{ws}k_B}, \tag{1}$$

is called "disorder-induced heating" (DIH). This is a nonequilibrium, ultrafast relaxation, similar to what occurs in high-density laser-produced plasmas and laser-driven fusion plasmas, as well as many other systems [14]. Interestingly, for the case of ultracold neutral plasmas, if the initial spatial distribution of ions was highly ordered and periodic this heating would not occur [5,15]. This suggests that DIH measurements could be used to measure disorder in systems such as BEC Mott insulators [16] and Rydberg crystals [17].

Plasma ions reach T_c approximately when $t\omega_p \sim 1$ [10,18–20], where $\omega_p = \sqrt{ne^2/m_i\epsilon_0}$ is the ion plasma frequency and m_i is the ion mass. This is a quasiuniversal behavior of dense plasma systems including Z-pinch and high-intensity laser ablation experiments when the the initial electrical potential energy is greater than the kinetic energy. The initial ion motion is dominated by nearest-neighbor interactions [18] when the ions push on each other. Even though single-particle motion in a plasma is tightly coupled to collective modes, collective motion does not begin until approximately one ion plasma

period (ω_p^{-1}) after DIH begins. Studies of DIH therefore necessarily explore the cross-over time that spans the transition from nearest-neighbor interactions to collective behavior.

Electrons screen interactions between ions in neutral plasmas. The typical screening distance is the Debye screening length, $\lambda_D = \sqrt{k_B T\epsilon_0/ne^2}$. When the Debye length λ_D is comparable to the distance between ions a_{ws}, screening reduces the ion-ion potential energy, slows the ion motion during the DIH phase, and reduces the final ion temperature.

The influence of electron screening on the ion temperature has been studied [10,18–20]. For systems in thermodynamic equilibrium, simulations of Yukawa fluids have found interaction energies and self-consistent temperatures displaying this effect [15,21–23]. Experimentally, studies have been published showing that the ion temperature scales with density as shown in Eq. (1) and that the DIH rise time scales as ω_p^{-1}. Figure 3 of [20] may suggest a change in the DIH time scale with density and temperature. However, no definitive studies or measurements of changes in the DIH process with electron screening appear to have been published.

In this paper we present a study of the density and temperature dependence of DIH in ultracold neutral plasmas. We measure this time using experimental measurements and computer simulations. Fluorescence is excited by passing a narrowband cw probe laser beam through the plasma. It is detuned a few linewidths from the ion resonance transition. The fluorescence signal is sensitive to the wings of the velocity distribution. We observe oscillations in the width of the ion velocity distribution and from this determine the time scale for the DIH process to occur. From the simulations we determine relationships between the electron screening parameter and the ion temperature and the rms velocity width. At high density and low temperature the observed DIH time scale departs from the expected $n^{-1/2}$ density scaling, and the role of electron screening in lengthening the DIH time scale is measured. We show how measuring the DIH time scale at known plasma density makes it possible to determine both the electron and ion temperatures 50 to 200 ns after the plasma is created.

II. METHODS

By combining experimental measurements with simulations we are able to relate observed signals to the details of

the ion velocity distribution. The details of the experiment and simulation are described in this section.

A. Experiment

In the experiment, 2×10^7 ^{40}Ca atoms are laser-cooled and trapped in a magneto-optical trap (MOT) [12]. The trap density is approximately $n(r) = n_0 \exp\left(-r^2/2\sigma^2\right)$, where $n_0 \leqslant 10(5) \times 10^{10}$ cm^{-3} and σ is 0.3 mm. Atoms in the trap are photoionized using pulsed lasers at 423 nm (the $4s^2\,^1S_0 \rightarrow 4s4p\,^1P_1$ transition) and 390 nm ($4s4p\,^1P_1 \rightarrow$ continuum) with pulse durations of 3 ns. The initial electron energy is typically determined by the wavelength of the 390-nm laser and is equal to the difference between the combined laser photon energy of the ionizing lasers and the atomic ionization potential. However, when the photon energy of the 390-nm pulsed laser ionizes the calcium atoms right at threshold the initial electron energy is determined by the bandwidth of the laser to approximately 1 cm$^{-1} \sim 0.5$ K.

After the plasma is generated, plasma ions are excited using a standing-wave cw probe laser beam detuned about four linewidths (a total of 90 MHz) below the $4s\,^2S_{1/2} \rightarrow 4p\,^2P_{1/2}$ transition at 397 nm. The probe laser beam is collimated to a Gaussian waist of 0.62 mm, making the rms size of the probe laser beam somewhat larger than the initial rms size of the ultracold plasma. The maximum probe laser beam intensity is approximately $s_0 = I/I_{\text{sat}} = 2$ times the saturation intensity, where $I_{\text{sat}} = 46$ mW/cm^2. Fluorescence at 397 nm is collected using a lens, isolated using a optical band-pass interference filter, detected using a 1-GHz bandwidth photomultiplier tube, and recorded using a 1-GHz bandwidth digital oscilloscope.

Sample fluorescence data are shown in Fig. 1. Ion fluorescence is plotted as a thin black line. The plasma is generated at time $t = 0$. The ground-state ions begin to scatter photons from the probe laser beam. A strongly damped Rabi oscillation in the ion population is visible near 7 ns. The time at which this signal maximizes depends on the probe laser beam detuning and intensity. This peak is followed by a broader shoulder in the fluorescence signal at 70 ns. The time at which this shoulder appears depends primarily on the plasma density and also on the electron temperature. This signal arises from broadening of the ion velocity distribution due to DIH, increasing the number of ions Doppler-shifted into resonance with the probe laser beam. At later times, the ion velocity distribution is further broadened by the outward radial acceleration and expansion of the plasma. This broadening gives rise to the very broad peak in the fluorescence signal at times near 1 μs, again depending on density and temperature.

The data analysis method is also shown in Fig. 1. The visibility of the DIH shoulder is increased by fitting the fluorescence signal in the 100-to-300-ns range to a straight line. This is shown as the dashed line in Fig. 1. The DIH peak in the background-subtracted signal, shown as the inset in Fig. 1, is fit using a parabola. The maximum of this parabolic fit is called t_0. It is an indicator of the time at which the width of the DIH-broadened velocity distribution reaches a maximum. As is shown in Sec. III, this time t_0 is offset a few percent from the time at which the velocity distribution reaches a local maximum.
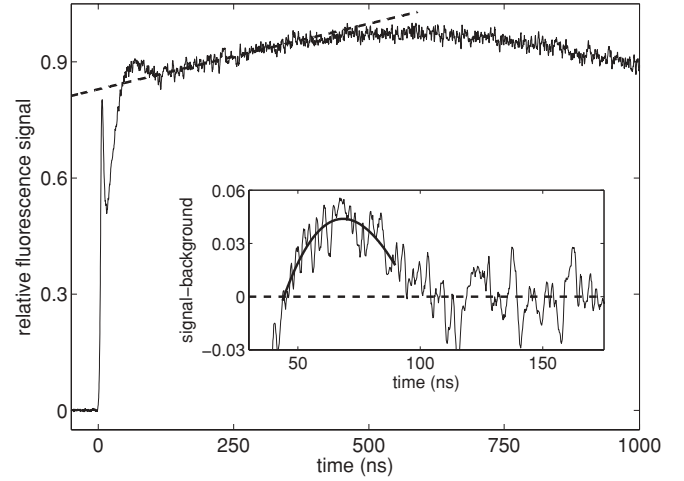

FIG. 1. Typical fluorescence signal and analysis, $T_e = 20$ K, $n_0 = 5 \times 10^{16}$ m^3, $\Delta f = -90$ MHz, and $s_0 = 1.7$. The fluorescence signal is plotted as a thin black line. The strongly damped Rabi oscillation gives a peak near 7 ns. The shoulder on the data near 70 ns is due to DIH broadening of the velocity distribution. The much broader signal peak near 600 ns is due to the accelerated expansion of the plasma. The heavy dashed line is a linear fit to the fluorescence signal between 100 and 300 ns. The inset shows the signal with this linear fit subtracted. The DIH signal now appears as a peak above a flat background. The heavy solid line shows a parabolic fit to the background subtracted data near the DIH peak. The time at which this fitted curve reaches its maximum is the characteristic DIH time, t_0.

B. Yukawa simulation

To better understand the experimental data and to test our data analysis, we simulate the fluorescence signal from the plasma. The simulation is described in Ref. [24]. It is performed by integrating the optical Bloch equations for a collection of ions in a cell. The ions interact via the Yukawa potential. The potential on ion j can be written as $\phi_Y = \sum_i e \exp\left(-r_{ij}/\lambda\right)/(4\pi\epsilon_0 r_{ij})$, where r_{ij} is the distance between plasma ions i and j, and the sum runs over all the ions in the cell with $i \neq j$. This treatment inherently assumes an isothermal electron distribution which is valid at early times as long as $\Gamma_e < 1$ [25].

Plasma ions are randomly distributed over a cubic cell with wrapped boundary conditions. The cell dimension is much smaller than the rms size of the plasma but larger than the Debye screening length. The ions move under the influence of the screened Coulomb force of the other ions in the cell. The force on ion j is $\vec{F}_j = -e\nabla_{ij}\phi_Y$, where the divergence is calculated with respect to the distance r_{ij}. This part of the simulation is similar to that of Ref. [18].

At each time step, we solve the optical Bloch equations for each ion in the cell. The fluorescence signal is proportional to the excited-state fraction. This fraction depends on the detuning of the laser beam from the 397-nm resonance transition for each ion. The detuning depends on the initial offset of the probe laser beam from the 397-nm resonance transition, on the ion motion due to DIH through the Doppler shift, and also on the overall accelerated plasma expansion. It has been shown that the plasma expansion at late times is
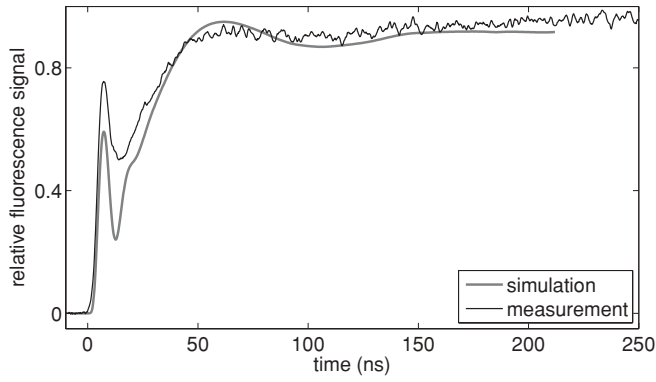
FIG. 2. A comparison of the simulated fluorescence signal (thick gray line) and the experimentally measured one (thin black line). Both signals show the heavily damped Rabi oscillation, the DIH shoulder, and the broad background due to the plasma expansion. For this plot the peak density is $n_0 = 5(3) \times 10^{10}$ cm^{-3}.

nontrivial when the initial electron temperature approaches T_C (or when the electron $\Gamma \approx 1$) [25].

However, as the details of the plasma expansion play a minor role during the first few hundred ns and we are careful to ensure the electron $\Gamma \ll 1$ in our simulation, the details of the expansion are relatively unimportant to our analysis. During the earliest part of the calculation we use $v(r,t) = r(2k_B T_e/m\sigma^2)t$ to calculate the velocity of the cell, where r is the radial coordinate of the cell. For times longer than ~ 50 ns we find the radial acceleration by solving the Gaussian expansion equations [26]. In this case, the size of the plasma σ increases with time.

A comparison of the simulated fluorescence data and the experimentally measured fluorescence data is shown in Fig. 2. Both signals show the heavily damped Rabi oscillation, the DIH shoulder, and the broad background due to the plasma expansion. The apparent height of the Rabi oscillation relative to the other fluorescence depends on the laser intensity and inhomogeneities in the experimental setup. However, the times at which these features appear agree well in the simulated and measured data over a wide range of density and temperature.

Using the simulation we can extract information about the plasma that is not easy to measure directly. This includes the details of the ion velocity distribution, the ion temperature as a function of time, and the influence of screening on ion equilibration.

III. DENSITY AND TEMPERATURE SCALING OF DIH IN A GAUSSIAN PLASMA

The temperature and density dependence of the DIH time t_0 is plotted in Fig. 3. Previous work has shown that the DIH time is proportional to the inverse of the nominal plasma frequency. Therefore, one would expect to find the relationship $t_0 \propto n^{-1/2}$. We see this density dependence at high temperatures and low densities, where the electron temperature is much greater than the correlation temperature T_C [see Eq. (1)] and the screening length λ_D is much greater than the mean distance between particles, a_{ws}. However, as the density increases and as the electron temperature approaches T_C, the time t_0 departs from the expected $n^{-1/2}$ density scaling. This departure is more
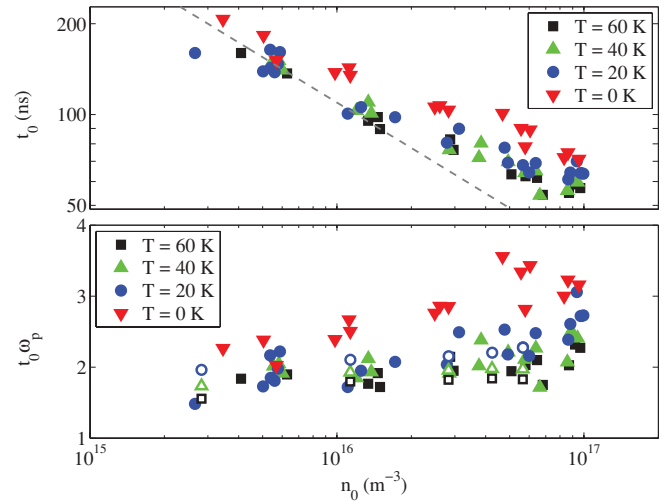

FIG. 3. (Color online) Experimental data. (Top) The time at which the DIH fluorescence peak occurs. The gray dashed line shows the expected time in the absence of screening effects. (Bottom) Scaled DIH peak time (data from the top panel) with t_0 corrected using Eq. (2). Open symbols are from the simulation. This data would all fall on a flat line if there was no screening.

apparent in the bottom panel of Fig. 3, where the quantity $t_0\omega_p$ is plotted as a function of density. If there was no screening effect, all of the data would fall on the same horizontal line near $t_0\omega_p \sim 1.5$.

It would be most valuable to connect the time t_0 to velocity distribution so that this time can be directly related to the true heating mechanism in the plasma. In the expanding Gaussian plasma simulation, we compare t_0 to the time at which the rms velocity distribution reaches its first maximum. We observe a small time difference. This difference, Δt, depends most strongly on density as

$$\Delta t = 22 \text{ ns} - (a_{ws})(7.7 \text{ ns}/\mu\text{m}). \quad (2)$$

For the densities in this study, this corresponds to a $\leqslant 15\%$ correction in the measured DIH peak time. This is much smaller than the factor of ~ 2 increase we see in the scaled time $t_0\omega_p$. We also see a dependence of Δt on the initial electron temperature. For the $T = 20$, 40, and 60 K data in this study, the temperature correction is an additional few percent. The correction in Eq. (2) is related to the difference between the width of the rms velocity distribution and the number of ions Doppler shifted into resonance with the probe laser beam. If the velocity distribution was exactly Gaussian, there would be no correction. However, the additional ions in the high-velocity tail of the distribution increases the fluorescence signal faster than the rms velocity distribution broadens. This difference is discussed briefly in Sec. IV A and Fig. 4.

The data in the top panel of Fig. 3, shows our measured t_0 as a function of density for a range of temperatures. In the bottom panel of Fig. 3 we plot the DIH peak time with the correction described in Eq. (2) applied and then multiplied by the nominal ion plasma frequency. The data clearly departs from a horizontal line as the temperature decreases and as the density increases. This observation shows the onset of many-body interactions in the ultracold plasma as the description of
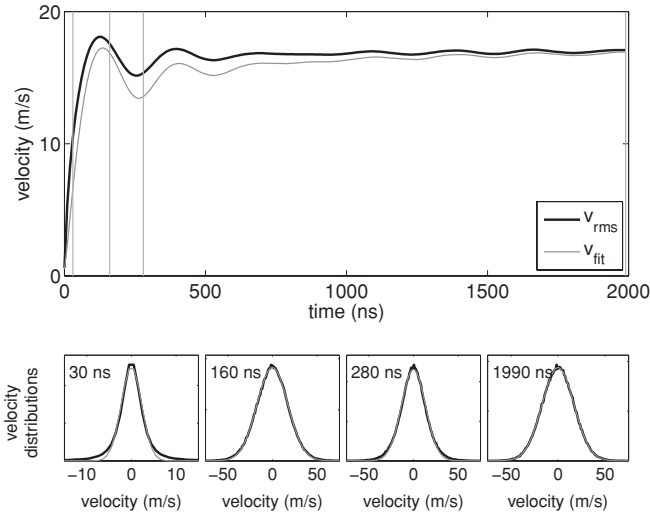
FIG. 4. Velocity distributions and their evolution with time. The top panel shows the rms velocity for $n = 4.0 \times 10^9$ cm^{-3} and an electron temperature of 60 K, plotted in the solid black line. Also plotted is the rms width of a Gaussian fit to the velocity distribution. High-energy ions in the wings of the distribution tend to make the rms width greater than the Gaussian width. The four vertical thin gray lines mark times at which the velocity distribution is plotted in the bottom four panels. The width changes in time, and the wings of the distribution show variations compared to the Gaussian fit. In these bottom four plots the black line is the distribution from the simulation and the gray lines are the best Gaussian fit to the distributions.

the ion motion changes from nearest-neighbor to many-body physics.

The data in Fig. 3 show t_0 measurements in plasmas with the initial $T_e = 0$ K. The DIH time lengthens out more in this case compared to the higher-temperature plasmas. This lowest possible initial temperature corresponds to ionizing the MOT atoms right at threshold. The electrons themselves experience DIH during the first few electron plasma periods, equilibrating to the correlation temperature. They slowly heat up during the next few hundred ns due to three-body recombination and electron-Rydberg scattering [26–28]. This is an interesting case because the density alone determines the electron and ion temperatures and even the plasma time scales.

Because the electron temperature is determined by the density through T_C the *electron* Γ_e should be about 1 for all densities [13,27]. A constant and density-independent value of the electron Γ_e also means that the inverse scaled screening length $\kappa = a_{ws}/\lambda_D \sim n^{1/6}/T^{1/2} \sim \sqrt{\Gamma_e}$ should be constant. In light of Eq. (7) (see Sec. IV D) one would therefore expect the scaled ion DIH time $t_0\omega_p$ to be constant. However, it is apparent that $t_0\omega_p$ is density-dependent. Future research is needed to determine if the observed changes in t_0 are intrinsic to the relaxation of the plasma ion velocity distribution or if they are related to effects described in Eq. (2).

IV. SIMULATIONS IN A UNIFORM-DENSITY PLASMA

To gain some insight into the relaxation of the plasma without the potentially confounding influence of the Gaussian spatial distribution and the accelerated plasma expansion, we present some data in this section from our simulation of a uniform plasma. The ions are still generated with random initial positions and interact via the Yukawa potential. Only the spatial distribution and plasma expansion are changed in this simulation.

A. Ion velocity distribution

First we present the evolution of the ion velocity distribution. During the DIH phase, the ion velocity distribution is non-Gaussian [18]. The initial ion motion is due to the electrostatic interaction of the (screened) ions. The nearest-neighbor distribution in the plasma gives rise to a nonthermal initial velocity distribution. This distribution relaxes over time and approaches a Boltzmann distribution.

A plot of the ion velocity distribution is shown in Fig. 4. The initial velocity distribution is Gaussian, corresponding to a thermal distribution at the 1 mK neutral atom temperature before the atoms are ionized. This distribution is quickly broadened due to DIH. Ions that are nearer to their neighbors experience greater initial accelerations and reach relatively high velocities. Compared to a thermal distribution, these ions overpopulate the wings of the distribution and contribute to a relatively high rms velocity. As shown in the top panel of Fig. 4, these high-velocity wings damp out on the time scale of 1000 ns as the ion velocity distribution thermalizes.

The bottom four panels of Fig. 4 show distributions at 30, 160, 280, and 1990 ns after the plasma is formed. The width of the distribution oscillates at early times. It is apparent from these plots that the rms velocity is skewed by the relatively few high-velocity ions. The oscillations in the distribution decay on the time scale of an oscillation period. However, some oscillations persist at long times. These oscillations can be used to extract the plasma frequency as discussed in the following paragraphs.

B. Plasma frequency and dispersion

In our uniform-density-plasma simulations, oscillations in the velocity distribution are visible at times beyond 1000 ns (as shown in the top panel of Fig. 4). These oscillations are a remnant of the initial hardening of the ion-ion potential that occurred when the plasma was created. It is as though the photoionization step gave a δ-function impulse to the system. The velocity oscillations at late times are a manifestation of the normal modes of the system.

One might expect the oscillation frequency to be equal to the nominal ion plasma frequency, $\omega_p = \sqrt{ne^2/m_i\epsilon_0}$. However, the ion-ion interaction is moderated by the electron screening. A simple one-dimensional model suggests how this screening might change the ion oscillation frequency. One can imagine two ions fixed in space at locations of $\pm a_{ws}$ on the x axis. A test charge of the same sign is also placed on the x axis, displaced a small distance x from the origin. In this model, the particles interact via the Yukawa potential with screening length λ_D, and the particles are constrained to move only along the x axis. The potential energy is quadratic for small displacements and has the form

$$U(x) = \frac{e^2}{4\pi\epsilon_0 a_{ws}^3}\left(1 + \kappa + \frac{\kappa^2}{2}\right)\exp(-\kappa)\, x^2, \qquad (3)$$

where $\kappa \equiv a_{ws}/\lambda_D$ is the inverse scaled screening length. The oscillation frequency of this harmonic oscillator is

$$\omega_{\text{model}} = \omega_p f(\kappa), \qquad (4)$$

where $f(\kappa) = \sqrt{2/3}(1 + \kappa + \kappa^2/2) \exp(-\kappa)$, ω_p is the ion plasma frequency, and the relationships between a_{ws}, n, and ω_p have been invoked. It is not expected that this oversimplified one-dimensional model will quantitatively predict the ion oscillation frequency. However, it hints at some of the important physics in the system and suggests that the frequency will get smaller as κ gets larger (corresponding to λ_D getting smaller).

We pursue the ion oscillation frequency just a little further here because it will help illustrate an important point about the DIH time t_0. We show that the ion oscillation frequency measured in our simulations agrees with previously published work under appropriate conditions. We also show that the characteristic DIH time t_0 in our simulations depends on κ but is *not* simply proportional to ω_p^{-1}.

The residual oscillations in the ion velocity distribution can be calculated using the dispersion relation. The dispersion relation gives the ion oscillation frequency as a function of screening length and mode wavelength. Dispersion relations for strongly coupled plasmas are reported in Ref. [29] for a wide range of ion and electron temperatures and plasma densities. Equation (7) in that paper,

$$\omega(q, \kappa) = \omega_p \left(\frac{q^2}{q^2 + \kappa^2} + \frac{q^2}{\Gamma} - \frac{\eta^{*2} q^4}{4} \right)^{1/2}, \qquad (5)$$

gives the real part of the ion plasma frequency and is appropriate for our plasmas. In this equation, $q \equiv k a_{ws} = 2\pi a_{ws}/\lambda$ is the scaled wave vector of the ion acoustic wave. Measurements probing the long-wavelength limit of the dispersion relation have recently been reported [30].

In our experiment, when an ultracold plasma is generated by ionizing the entire plasma, a wave packet is launched through the plasma. The average mode frequency can be obtained by averaging over an appropriate range of q values in Eq. (5). In essence, q becomes a fit parameter for our data, and Eq. (5) tells us how the average ion oscillation frequency changes with the screening length, κ.

These results are compared to Eq. (5) in Fig. 5. We use the ion temperature from in the simulation at times later than 1000 ns to calculate the ion Γ. We use the initial electron temperature and density to calculate κ. The best match of the data to the dispersion curve occurs with $q = 0.55$. We find a similarly good match by averaging Eq. (5) when q ranges from 0 to about 1.

C. t_0 and the ion oscillation frequency

With the average ion oscillation frequency in hand, we can show that the DIH time t_0 is not related either to this frequency or to the ion plasma frequency ω_p. The first DIH maximum in the ion velocity distribution width occurs when the initially stationary ions accelerate away from each other and before they collide with other neighboring ions. If this was a plasma oscillation, one could calculate the oscillation frequency ω by assuming that $t_0 \omega = \pi/2$. In Fig. 5 the frequency obtained in
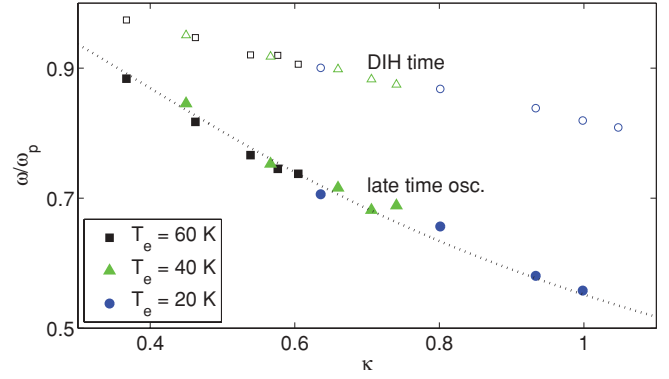

FIG. 5. (Color online) The ion oscillation frequency as a function of the inverse scaled screening length κ in a uniform (simulated) plasma. The solid symbols show the frequency determined from late-time ion velocity oscillations. The dashed line is Eq. (5) with $q = 0.55$. The open symbols show the ion oscillation frequency calculated by assuming that the DIH peak occurs $\frac{1}{4}$ through the oscillation period.

this manner is plotted as a function of κ, represented as open symbols.

This frequency is clearly not the ion plasma frequency $\sqrt{ne^2/m_i \epsilon_0}$ because our observed "frequency" depends on κ. It is also clearly not the average mode frequency. There are no physically relevant values of either Γ or q that reproduce the observed dependence on κ.

This is perhaps not surprising. The relaxation of the plasma begins when there is no true thermodynamic equilibrium. As the system thermalizes, the plasma mode description becomes more appropriate. Interestingly, the changes in DIH time predicted by nearest-neighbor models is much weaker than what we observe in Fig. 5. It is clear, therefore, that the DIH time spans the crossover from a regime in which nearest-neighbor interactions dominate ion motion to one in which many-body physics is appropriate.

D. Ion temperature and DIH time in a uniform-density plasma

In the simulations, the equilibrium ion temperature depends on κ. In the simulation we can extract the rms ion velocity at times beyond 1000 ns after the initial transient oscillations have damped out. From this we can determine the ion temperature. We observe that the equilibrium ion temperature depends on the electron screening parameter as

$$\Gamma = 2.490 + 0.929\kappa + 0.785\kappa^2. \qquad (6)$$

The DIH time t_0 also depends on on κ. The relationship is

$$t_0 \omega_p = 1.445 + 0.467\kappa. \qquad (7)$$

These equations are valid for $0.3 < \kappa < 1$.

In a plasma with known density, the DIH time can be measured and Eqs. (6) and (7) can be used to first determine κ and then to determine Γ. Both the electron and the ion temperature can be determined by measuring only t_0. Because the ion velocity distribution does not change significantly after t_0, this determination gives the temperatures at early times in the plasma, as short as 50 ns after the plasma is generated. Future work could test whether this continues to be true when the electrons become strongly coupled or when three-body

recombination and electron-scattering become important in very-low-temperature (or high-density) plasmas.

V. CONCLUSION

In conclusion, we have presented measurements and simulations of laser-induced fluorescence from ultracold neutral plasmas. We measure the time scale over which DIH occurs for a range of densities and temperatures. The DIH time departs from the expected $n^{-1/2}$ density scaling at high densities. It also depends on temperature. We use a simulation to determine the relationship between the observed DIH time and the first maximum in the rms velocity distribution. The DIH time depends on the electron screening length and it spans the transition from a nearest-neighbor to a many-body description of the system. Understanding this dynamic nonequilibrium transition may provide insights into other transient phenomena in laser physics and other applications.

Our simulation shows that the DIH time can be used to calculate the electron and ion temperatures in ultracold neutral plasmas approximately 100 ns after the plasma is created. This reduces the earliest time measurements of electron temperature for these systems. Further research could test these relationships [Eqs. (6) and (7)] when $\kappa > 1$ where recombination and scattering effects may be important at these early times. Additional research is also required to study the relationship between the fluorescence signal, which probes the wings of the velocity distribution, and the first maximum in the width of the velocity distribution. These future studies will require full molecular dynamics simulations because the Yukawa approximation is expected to be invalid in this regime.

ACKNOWLEDGMENTS

[1] T. C. Killian and S. D. Bergeson, Phys. World, February 2003, p. 37.

[2] T. C. Killian, Science **316**, 705 (2007).

[3] S. L. Rolston, Physics **1**, 2 (2008).

[4] T. C. Killian and S. L. Rolston, Phys. Today **63**, 46 (2010).

[5] T. Killian, T. Pattard, T. Pohl, and J. Rost, Phys. Rep. **449**, 77 (2007).

[6] M. Bonitz, C. Henning, and D. Block, Rep. Prog. Phys. **73**, 066501 (2010).

[7] T. C. Killian, S. Kulin, S. D. Bergeson, L. A. Orozco, C. Orzel, and S. L. Rolston, Phys. Rev. Lett. **83**, 4776 (1999).

[8] S. Kulin, T. C. Killian, S. D. Bergeson, and S. L. Rolston, Phys. Rev. Lett. **85**, 318 (2000).

[9] T. C. Killian, M. J. Lim, S. Kulin, R. Dumke, S. D. Bergeson, and S. L. Rolston, Phys. Rev. Lett. **86**, 3759 (2001).

[10] Y. C. Chen, C. E. Simien, S. Laha, P. Gupta, Y. N. Martinez, P. G. Mickelson, S. B. Nagel, and T. C. Killian, Phys. Rev. Lett. **93**, 265003 (2004).

[11] C. E. Simien, Y. C. Chen, P. Gupta, S. Laha, Y. N. Martinez, P. G. Mickelson, S. B. Nagel, and T. C. Killian, Phys. Rev. Lett. **92**, 143001 (2004).

[12] E. A. Cummings, J. E. Daily, D. S. Durfee, and S. D. Bergeson, Phys. Rev. Lett. **95**, 235001 (2005).

[13] S. G. Kuzmin and T. M. O'Neil, Phys. Rev. Lett. **88**, 065003 (2002).

[14] M. S. Murillo, J. Phys. A **42**, 214054 (2009).

[15] M. S. Murillo, Phys. Rev. Lett. **87**, 115003 (2001).

[16] M. Greiner, O. Mandel, T. Esslinger, T. W. Hansch, and I. Bloch, Nature (London) **415**, 39 (2002).

[17] T. Pohl, E. Demler, and M. D. Lukin, Phys. Rev. Lett. **104**, 043002 (2010).

[18] M. S. Murillo, Phys. Rev. Lett. **96**, 165001 (2006).

[19] S. Laha, Y. C. Chen, P. Gupta, C. E. Simien, Y. N. Martinez, P. G. Mickelson, S. B. Nagel, and T. C. Killian, Eur. Phys. J. D **40**, 51 (2006).

[20] J. Castro, P. McQuillen, H. Gao, and T. C. Killian, J. Phys. Conf. Ser. **194**, 012065 (2009).

[21] R. T. Farouki and S. Hamaguchi, J. Chem. Phys. **101**, 9885 (1994).

[22] S. Hamaguchi, R. T. Farouki, and D. H. E. Dubin, J. Chem. Phys. **105**, 7641 (1996).

[23] S. Hamaguchi, R. T. Farouki, and D. H. E. Dubin, Phys. Rev. E **56**, 4671 (1997).

[24] A. Denning, S. D. Bergeson, and F. Robicheaux, Phys. Rev. A **80**, 033415 (2009).

[25] P. Gupta, S. Laha, C. E. Simien, H. Gao, J. Castro, T. C. Killian, and T. Pohl, Phys. Rev. Lett. **99**, 075005 (2007).

[26] F. Robicheaux and J. D. Hanson, Phys. Rev. Lett. **88**, 055002 (2002).

[27] S. G. Kuzmin and T. M. O'Neil, Phys. Plasmas **9**, 3743 (2002).

[28] S. Mazevet, L. A. Collins, and J. D. Kress, Phys. Rev. Lett. **88**, 055001 (2002).

[29] H. Ohta and S. Hamaguchi, Phys. Rev. Lett. **84**, 6026 (2000).

[30] J. Castro, P. McQuillen, and T. C. Killian, Phys. Rev. Lett. **105**, 065004 (2010).